Journal of Power Sources 391 (2018) 170–179

Contents lists available at ScienceDirect

Journal of Power Sources

journal homepage: www.elsevier.com/locate/jpowsour

Cold sintering and ionic conductivities of $Na_{3.256}Mg_{0.128}Zr_{1.872}Si_2PO_{12}$ solid electrolytes

Haoyang Leng, Jiajia Huang, Jiuyuan Nie, Jian Luo*

Department of NanoEngineering, Program of Materials Science and Engineering, University of California, San Diego, 9500 Gilman Drive, La Jolla, CA 92093-0448, USA

HIGHLIGHTS

- The cold sintering process (CSP) densifies NASICON specimens at 140 °C.
- With identical heat treatments, CSP leads to > 2-6X increases in conductivities.
- Post-CSP annealing at 800 °C markedly increases the grain boundary conductivity.
- Mg doping enhances the densification and conductivity of cold-sintered specimens.
- A new opportunity of low-T sintering of solid electrolytes and solid-state batteries.

ARTICLE INFO

Keywords:
Cold sintering process
NASICON
Ionic conductivity
Solid-state battery
Sodium-ion battery

ABSTRACT

The recent invention of cold sintering process (CSP) suggests a new opportunity to densify ceramic solid electrolytes at reduced temperatures. In the study, $Na_{3.256}Mg_{0.128}Zr_{1.872}Si_2PO_{12}$ (Mg-doped NASICON) specimens were cold-sintered at 140 °C to ~83% of the theoretical density. In addition, post-CSP annealing, at temperatures lower than that is needed for the conventional sintering of NASICON, can substantially increase the ionic conductivity (with or without significant further densification). For example, the conductivity of cold-sintered Mg-doped NASICON reached > 0.5 mS/cm after annealing at (as low as) 800 °C; in comparison, a dry-pressed specimen exhibited virtually no densification at a higher temperature of 1000 °C with < 0.1 mS/cm conductivity. Moreover, a high conductivity of ~1.36 mS/cm has been achieved for a Mg-doped NASICON cold-sintered and subsequently annealed at 1100 °C (doubling the conductivity of a dry-pressed specimen sintered at the identical condition). Further mechanistic studies showed that annealing at 800–1100 °C increased the grain boundary (GB) conductivities of cold-sintered specimens. The CSP opens a new window to sinter the "thermally-fragile" ceramic solid electrolytes (such as phosphates and sulfates). In addition, it not only provides energy and cost savings but also enables new fabrication routes to make solid-state batteries.

1. Introduction

Recently, the research of sodium-ion batteries has gained great attentions due to the abundant sodium resources and its lower cost in comparison to lithium [1–5]. Furthermore, the development of solid-state batteries has also attracted significant interests in both the academe and the industry, where solid electrolytes, instead of liquid electrolytes that are prone to the leakage, dendrite growth, and explosion risks, are used to improve safety and (potentially) energy density (e.g., via enabling the use of metal anodes) [6–8]. Specifically, solid-state sodium batteries can in principle have low costs and possess high energy density for large-scale energy storage applications, such as those used in power grids [8]. Here, one key enabling technology is to cost-effectively fabricate sodium-ion solid electrolytes with high conductivity and stability [8–11].

Specifically, solid-state sodium batteries with natrium (Na) superionic conductors (NASICON) were demonstrated to be promising energy storage devices [8,12]. Recently, solid-state batteries with NASICON based composite polymer electrolytes have also been designed and fabricated, which exhibited high specific capacity and stable cycle performance [13–15]. The NASICON materials with the general formula of $Na_{1+x}Zr_2Si_xP_{3-x}O_{12}$ ($0 \le x \le 3$) were firstly developed by Hong and Goodenough ~40 years ago [16,17]. The Na^+ ionic conductivities of NASIOCN ceramic electrolytes are relative high compared to other inorganic solid electrolytes at elevated temperatures [18,19]. In addition, NASICON ceramic electrolytes possess a wide

* Corresponding author.
E-mail address: jluo@alum.mit.edu (J. Luo).

https://doi.org/10.1016/j.jpowsour.2018.04.067
Received 28 February 2018; Received in revised form 16 April 2018; Accepted 19 April 2018

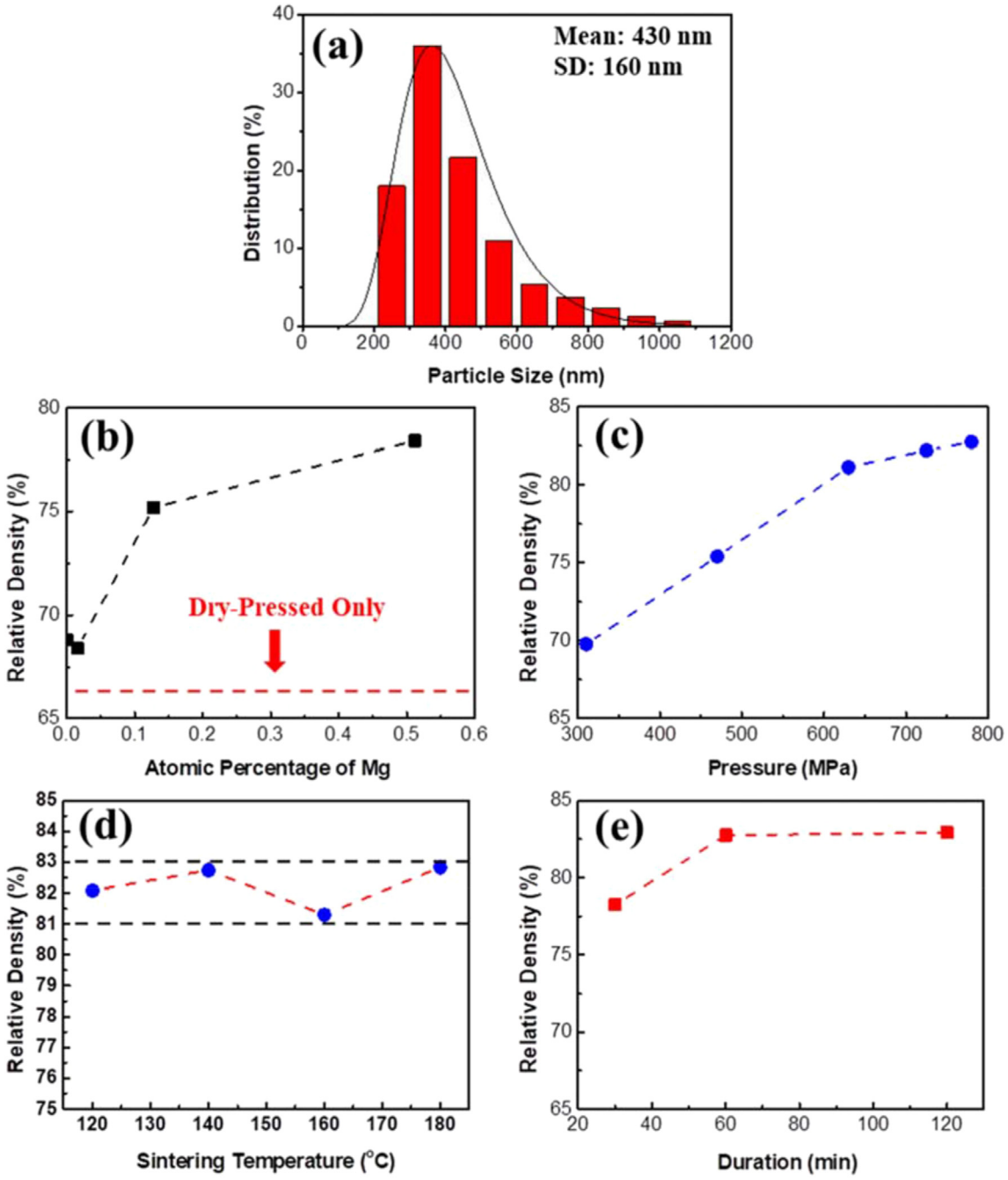

Fig. 1. (a) Measured particle size distribution of the synthesized Mg-doped NASICON powder (where the solid curve represents a lognormal fitting). **(b)** Relative density vs. Mg atomic percentage curve for NASICON specimens cold-sintered at 140 °C for 1 h under a fixed pressure of 470 MPa. **(c)** Relative density vs. applied pressure curve for Mg-doped NASICON ($Na_{3.256}Mg_{0.128}Zr_{1.872}Si_2PO_{12}$) specimens cold-sintered at a fixed temperature of 140 °C and a fixed holding duration of 1 h. **(d)** Relative density vs. sintering temperature curve for $Na_{3.256}Mg_{0.128}Zr_{1.872}Si_2PO_{12}$ specimens cold-sintered at a fixed pressure of 780 MPa and a fixed holding duration of 1 h. **(e)** Relative density vs. annealing duration curves for $Na_{3.256}Mg_{0.128}Zr_{1.872}Si_2PO_{12}$ specimens cold-sintered at a fixed temperature of 140 °C and a fixed pressure of 780 MPa. The estimated errors of measured densities are ± 1.5%. 30 wt % water was added in each cold-sintered specimen.

electrochemical window, high Na ion transference numbers, and high thermal stability [14,15,19,20]. NASICON oxides are more air and moisture stable than sulfides [12–15]. However, undoped NASICONs typically have moderate total, i.e., bulk plus grain boundary (GB), ionic conductivities at room temperature (~0.1 mS/cm) due to the poorly-conducting ZrO_2 phases precipitated at GBs during the high-temperature (typically ~1200 °C) sintering [16–20]. Recently, aliovalent doping has been reported to increase the ionic conductivities of NASICON by several different groups independently [21–25]. In one study, Samiee et al. reported that the 0.128 at. % Mg doped NASICON can exhibit a high ionic conductivity around 2 mS/cm at room temperature (with the optimal sintering process) [21]; furthermore, a careful combined experimental and modeling investigation contributed the enhanced conductivity to the formation of a conductive secondary and/or interfacial Na_3PO_4 phase at GBs, representing one example with a clear explanation of underlying mechanisms of the so-called "doping" effects (that are in fact more of interfacial and microstructural, than the bulk, effects) [21].

However, the high processing temperatures (typically 1200 °C or higher) and long durations of NASICON materials in conventional

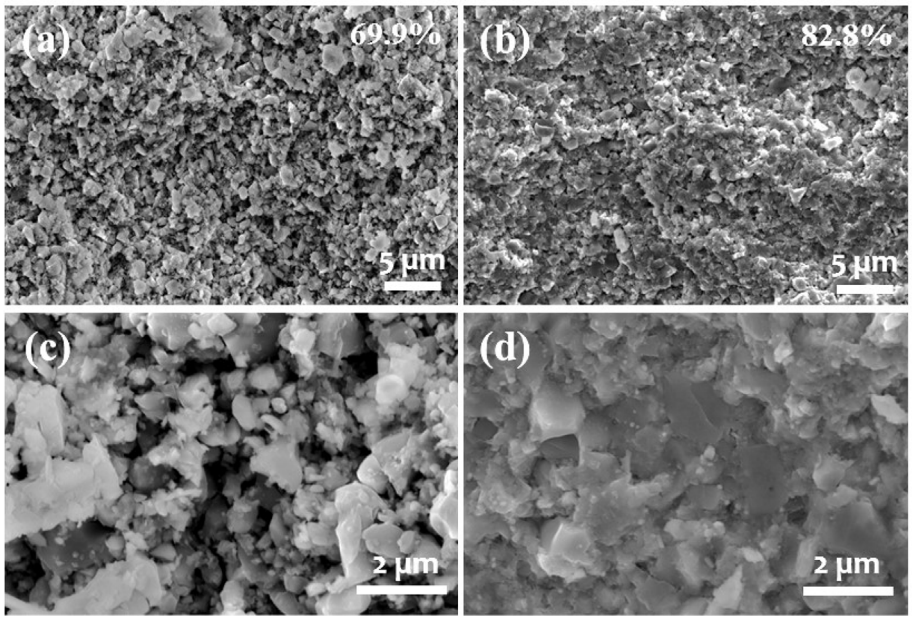

Fig. 2. SEM micrographs of the fractured surfaces of Mg-doped NASICON ($Na_{3.256}Mg_{0.128}Zr_{1.872}Si_2PO_{12}$) specimens **(a, c)** dry-pressed at 25 °C and **(b, d)** cold-sintered at 140 °C, respectively, both at 780 MPa for 1 h.

sintering can cause the Na and P evaporation, which results in the formation of insulating ZrO_2 secondary phase at GBs to lower the ionic conductivity [26,27]. The poor sinterability of NASICON and required prolonged sintering at ≥1200 °C also add significant costs and energy consumption, as well as cause various technical and compatibility issues to make it more difficult to fabricate thin NASICON membranes and/or integrate them into solid-state battery technologies, particularly for mass production of grid- (or other large-) scale energy storage devices. Thus, there are great technological advantages to explore novel sintering technologies to reduce the sintering or heat treatment temperatures of NASICON materials, motivating this study.

Recently, an innovative ceramic processing technology, cold sintering process (CSP), was developed by researchers at Pennsylvania State University, which densifies ceramics with the assistance of an aqueous solution at a temperature below 300 °C for a short duration (typically 15–60 min) under an uniaxial pressing pressure (100–500 MPa) [28]. In the CSP, the initial densification is likely caused by particle rearrangements under the applied pressure with the assistance of the aqueous solution among particles, where dissolution is promoted. Subsequently, a supersaturated solution forms among particles and a dissolution-precipitation process occurs to provide mass transport (densification) at a moderate temperature under the applied pressure, while the water gradually evaporates [28]. In many (most) cases, a post-CSP annealing is still needed to achieve the final property requirements, but it can be conducted at a temperature lower that is required for conventional sintering of dry-pressed specimens, thereby providing a technological advantage. In the last a couple of years, the CSP has been applied to densify a spectrum of functional ceramics and ceramic-polymer composites, including ZnO [29], $BaTiO_3$ [30], ZrO_2 [31,32], KH_2PO_4 [33], V_2O_5 based composites [34], and $LiFePO_4$ [35]. Specially, Berbano et al. demonstrated that the CSP could densify $Li_{1.5}Al_{0.5}Ge_{1.5}(PO_4)_3$ (LAGP) solid electrolytes to around 80% of the theoretical density at 120 °C for 20 min, but post-CSP annealing is needed to increase their conductivity [36].

In this work, we further apply the CSP to a Mg-doped NASICON ($Na_{3.256}Mg_{0.128}Zr_{1.872}Si_2PO_{12}$) and successfully achieved ~83% of the theoretical density at as low as 140 °C for 1 h. Similar to LAGP [36], post-CSP annealing (at temperatures lower than the conventional sintering temperature) was found to be necessary and effective to increase the ionic conductivity of cold-sintered NASICON; moreover, our further mechanistic study showed that the increased conductivity was achieved by reducing the high GB resistance in the as-CSP specimens. Specifically, this study has demonstrated that the CSP can lead to a > 2-6X increase in the conductivity in comparison with the conventional (dry-pressed) specimen sintered at the identical (reduced) temperature for an identical duration. Thus, this study suggests a promising new opportunity for applying the CSP to fabricate solid-state electrolytes and batteries.

2. Experimental

2.1. Powder synthesis

The NASICON powders with the compositions of $Na_{3.256}Mg_{0.128}Zr_{1.872}Si_2PO_{12}$ (Mg-doped NASICON) and $Na_3Zr_2Si_2PO_{12}$ (undoped NASICON) were synthesized by a solid-state reaction method using stoichiometric amounts of Na_2CO_3 (Fisher Chemical, 99.5%), MgO (Alfa Aesar, 99.95%), ZrO_2 (Fisher Chemical, Laboratory Grade), SiO_2 (Alfa Aesar, 99.9%), and $NH_4H_2PO_4$ (Sigma Aldrich, 99.99%). Noting that we also made several other NASICON specimens with different Mg contents that are reported in Fig. 1(b), but all other Mg-doped NASICON specimens reported and discussed elsewhere have the composition $Na_{3.256}Mg_{0.128}Zr_{1.872}Si_2PO_{12}$. The mixtures were milled in isopropyl alcohol using a planetary ball mill for 24 h. The mixed precursors were dried in an oven at 85 °C for 12 h and subsequently calcinated in air at 1150 °C for 5 h. Finally, the calcined powders were again ball milled in isopropyl alcohol for 48 h to decrease the particle sizes.

2.2. Cold sintering process (CSP) and Post-CSP treatments

The CSP powders were prepared by mixing the (Mg-doped or undoped) NASICON powder with 30 wt % deionized (DI) water in mortar and pestle for 2–3 min. The prepared powder was transferred into a die (with a diameter of ¼ inch) and uniaxially pressed at 780 MPa at room temperature (25 °C) for 2 min for a pre-pressing step. Then, the die was heated to a preset CSP temperature (140 °C in most cases) with a heating tape (wrapped around the die) using a temperature controller. The specimen was kept at this CSP temperature (e.g., 140 °C) for a fixed duration (typically 1 h) at a fixed pressure (typically 780 MPa). We also

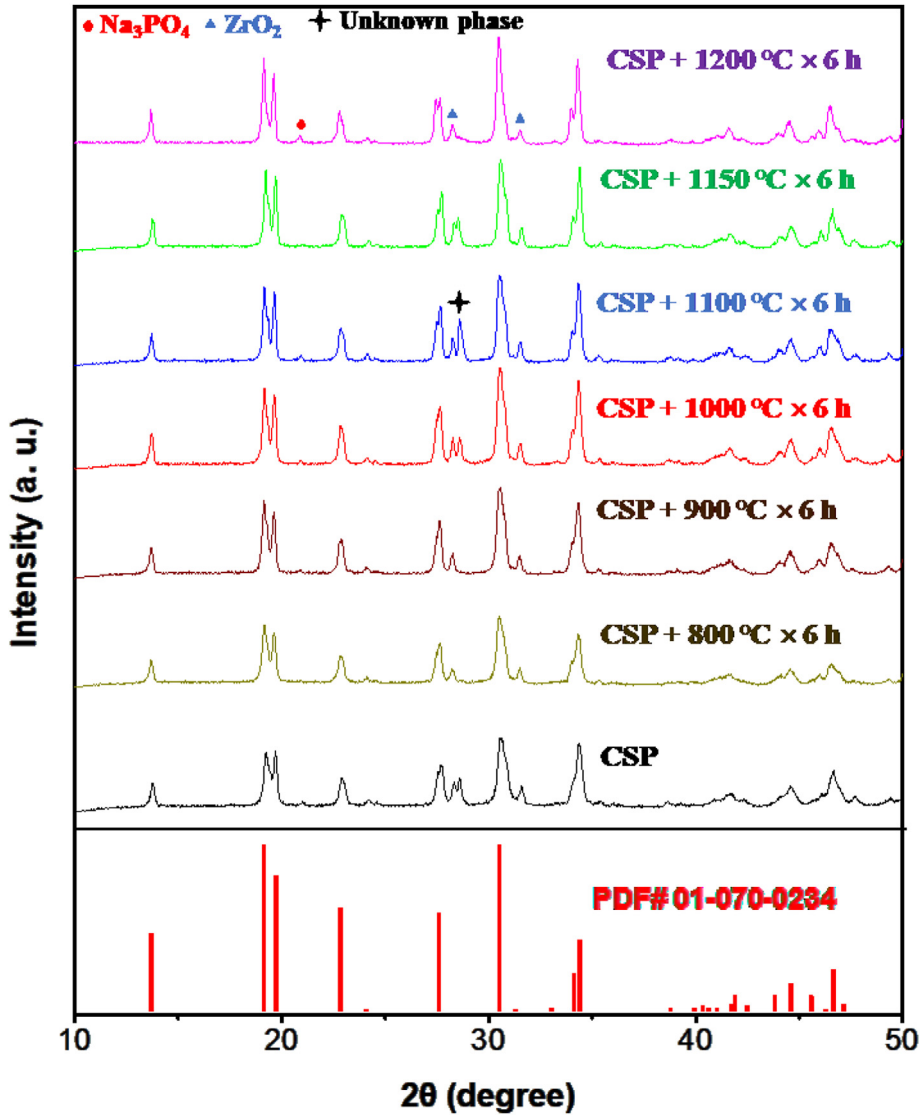

Fig. 3. XRD patterns of the Mg-doped NASICON ($Na_{3.256}Mg_{0.128}Zr_{1.872}Si_2PO_{12}$) specimens after CSP only (i.e., an as-cold-sintered specimen) and CSP plus subsequent annealing at six different temperatures, along with the reference $Na_3Zr_2Si_2PO_{12}$ pattern (PDF No. 01-070-0234).

studied the effects of varying the CSP temperature (120–180 °C), duration (10–120 min), and pressure (300–780 MPa). All cold-sintered specimens were baked at 200 °C for 12 h to remove any residual moisture.

Most cold-sintered specimens were subsequently annealed at 600–1200 °C for 6–48 h in a box furnace with a heating ramp rate of 5 °C/min. For comparison, conventional dry-pressed NASIOCN specimens were also prepared by using the identical pressure (780 MPa) at room temperature and subsequently sintered (a.k.a. annealed) at identical temperatures for identical durations.

2.3. Characterization and measurements

The specimen densities were obtained by measuring the mass and dimensions of each specimen and the theoretical density of NASICON is ~3.27 g/cm^3. The crystalline phases of samples were identified by X-ray diffraction (XRD) using a Rigaku diffractometer with Cu K_α radiation. The scanning electron microscopy (SEM, FEI Quanta 250) was used to observe the microstructures of fractured surfaces.

The specimens for conductivity measurements were prepared by sputtering Pt blocking electrodes on both surfaces of the pellets. The thicknesses of all the specimens were in the range of 1.0–1.3 mm. Electrochemical impedance spectroscopy (EIS) was carried out by using a Solartron 1255B EIS analyzer in the frequency range from 10^6 to 1 Hz with AC amplitudes of 25, 50, or 75 mV to measure the conductivity at room temperature (25 °C) or controlled low temperatures. The conductivity measurements were also carried out at 0 °C, −20 °C, −40 °C, −60 °C, respectively, in a cold chamber with a temperature controller (LR Environmental Equipment Company) in dry air. The GB, bulk, and total ionic conductivities were obtained by fitting Nyquist plots using the Z-View software (Scribner, Inc.). A DC polarization test (with an applied voltage of 1V at room temperature) was conducted to measure the sodium ion transference number by following the reported standard procedure [19,20]. The conductivity was continuously measured until the current was stabilized. The tested $Na_{3.256}Mg_{0.128}Zr_{1.872}Si_2PO_{12}$ specimen (CSP + 1100 °C × 48 h) was prepared by sputtering Pt electrodes on both surfaces of the pellet (dimension: ~1.2 mm thick and 6.0 mm in diameter).

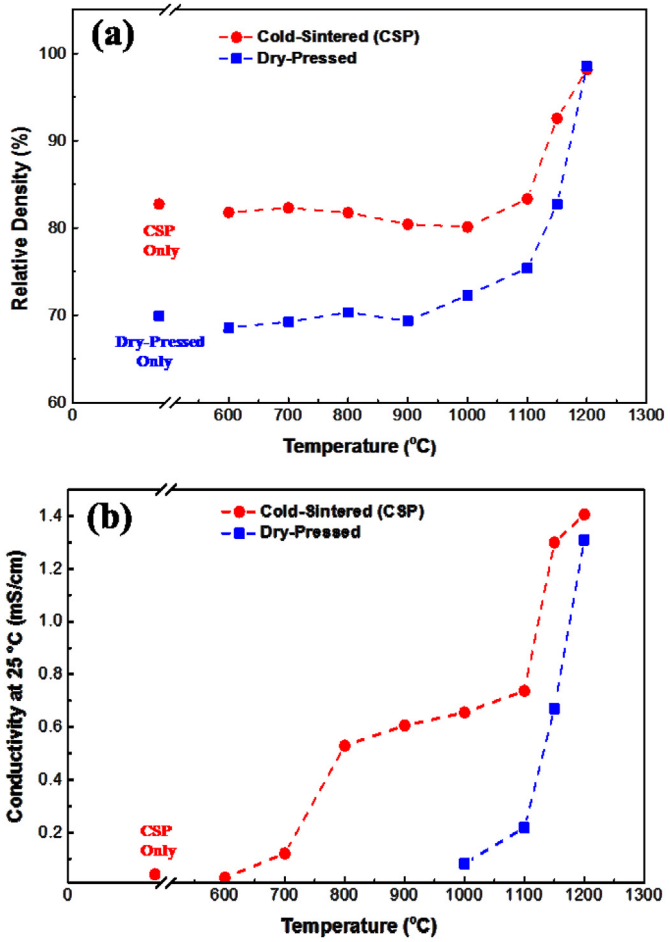

Fig. 4. The **(a)** relative density and **(b)** total ionic conductivity (measured at room temperature) of the cold-sintered and dry-pressed Mg-doped NASICON ($Na_{3.256}Mg_{0.128}Zr_{1.872}Si_2PO_{12}$) specimens vs. annealing temperature curves. All cold-sintered and dry-pressed specimens were annealed for 6 h.

3. Results and discussion

3.1. Cold sintering: effects of the Mg content and CSP parameters on densification

The particle size distribution of the synthesized Mg-doped NASICON powders was obtained by SEM analysis and are shown in Fig. 1(a); the mean particle size was measured to be 430 nm, with a standard deviation of 160 nm. Fig. 1 further shows the effects of the Mg content and CSP pressure, temperature, and duration (holding time) on the densification of NASICON materials. As shown in Fig. 1(b), Mg doping can substantially increase the densification of NASICON. On one hand, the CSP with 30 wt % water at 140 °C for 60 min was found ineffective to densify the undoped NASICON; it resulted in a relative density of ~68.8%, which is only slightly higher than the ~66.2% relative density achieved by dry pressing a specimen at the identical pressure of 470 MPa. On the other hand, 0.128 at. % Mg doping increased the relative density to > 75% at 470 MPa, and 0.512 at. % Mg doping further increased it to > 78%. To explain this observation, we should note that the enhanced densification in cold sintering must be enabled by the solubility of the solid phase(s) in water [28]. It is known that the NASICON type electrolytes are relative stable in water at 60 °C, suggesting limited solubilities [37,38]; however, it is yet unknown whether a higher temperature and a higher pressure can promote more solubility to enable cold sintering. A prior study showed that Mg doping could lead to the formation of conductive Na_3PO_4 secondary and/or interfacial phase [21] that has high solubilities in water, which may promote cold sintering. Moreover, Mg doping can also promote a transformation of primary NASICON from the monoclinic to the rhombohedral phase [21], which may also be a factor that changes the solubility and cold sintering kinetics. Further studies are needed to investigate the exact underlying mechanisms.

Table 1
Measured room-temperature total conductivity for undoped ($Na_3Zr_2Si_2PO_{12}$) and Mg-doped ($Na_{3.256}Mg_{0.128}Zr_{1.872}Si_2PO_{12}$) NASICON specimens that were either cold-sintered or dry-pressed and subsequently annealed at different temperatures for different durations. All CSP specimens shown here were cold-sintered at 140 °C and 780 MPa for 1 h.

Specimen	Processing Condition	σ_t (mS/cm)	Relative Density (%)
Mg-doped	CSP only	0.041	82.9
Mg-doped	CSP + 600 °C × 6 h	0.028	81.8
Mg-doped	CSP + 700 °C × 6 h	0.12	82.3
Mg-doped	CSP + 800 °C × 6 h	0.529	81.8
Mg-doped	Dry-Pressed (140 °C × 1 h) + 800 °C × 6 h	0.075	72.4
Mg-doped	Dry-Pressed (RT) + 800 °C × 6 h	0.061	70.3
Mg-doped	CSP + 900 °C × 6 h	0.606	80.4
Undoped	CSP + 900 °C × 6 h	0.267	77.3
Mg-doped	CSP + 1000 °C × 6 h	0.655	80.2
Mg-doped	Dry-Pressed (RT) + 1000 °C × 6 h	0.082	72.3
Mg-doped	CSP + 1100 °C × 6 h	0.737	83.3
Mg-doped	Dry-Pressed (RT) + 1100 °C × 6 h	0.218	75.4
Mg-doped	CSP + 1100 °C × 12 h	0.878	86.9
Mg-doped	Dry-Pressed (RT) + 1100 °C × 12 h	0.28	76.5
Mg-doped	CSP + 1100 °C × 24 h	1.013	88.9
Mg-doped	Dry-Pressed (RT) + 1100 °C × 24 h	0.388	80.2
Mg-doped	CSP + 1100 °C × 48 h	1.362	93.6
Mg-doped	Dry-Pressed (RT) + 1100 °C × 48 h	0.601	82.3
Undoped	CSP + 1100 °C × 48 h	0.506	91.6
Mg-doped	CSP + 1150 °C × 30 min	0.78	86.7
Mg-doped	Dry-Pressed (RT) + 1150 °C × 30 min	0.219	74.1
Mg-doped	CSP + 1150 °C × 1 h	1.045	89.2
Mg-doped	Dry-Pressed (RT) + 1150 °C × 1 h	0.261	79.9
Mg-doped	CSP + 1150 °C × 6 h	1.3	92.6
Mg-doped	Dry-Pressed (RT) + 1150 °C × 6 h	0.67	82.7
Mg-doped	CSP + 1150 °C × 12 h	1.45	94.3
Mg-doped	Dry-Pressed (RT) + 1150 °C × 12 h	0.876	87.1
Mg-doped	CSP + 1150 °C × 24 h	1.182	93.8
Mg-doped	Dry-Pressed (RT) + 1150 °C × 24 h	0.851	87.9
Mg-doped	CSP + 1200 °C × 6 h	1.406	98.1
Mg-doped	Dry-Pressed (RT) + 1200 °C × 6 h	1.31	98.6

Although a higher Mg content can further increase the densification of NASICON in the CSP, 0.128 at. % Mg doped NASICON was chosen for our systematic CSP experiments because of its optimal conductivity (as a higher Mg content can lead to a phase transformation of the primary NASICON phase from the high-conducting monoclinic to the low-conducting rhombohedral phase, according to a prior study [21]).

Fig. 1(c) shows the increasing densification with increasing pressure for the CSP of Mg-doped NASICON ($Na_{3.256}Mg_{0.128}Zr_{1.872}Si_2PO_{12}$) at the sintering temperature 140 °C for 1 h. Specifically, the specimen cold-sintered at 310 MPa has a relative density ~69.8% and a high relative density of ~82.8% was achieved at 780 MPa. Thus, the applied pressure of 780 MPa was used in the subsequent CSP experiments. Furthermore, Fig. 1(d) shows the CSP temperature (in the range of 120–180 °C) have little influence on the final density; the subsequent CSP experiments were conducted at 140 °C. Finally, Fig. 1(e) shows the density variation with the CSP duration; the relative density increased from a duration (hold time) of 30–60 min, but it did not increase further for an even longer duration of 120 min, presumably because the water was dried after ~60 min. We also note that baking of the 60-min cold-sintered specimen at 200 °C for 12 h resulted in no weight loss, indicating that it was dried. Hence, the subsequent CSP experiments were conducted for a fixed duration of 60 min (or 1 h).

In summary, a high relative density of ~83% has been achieved for

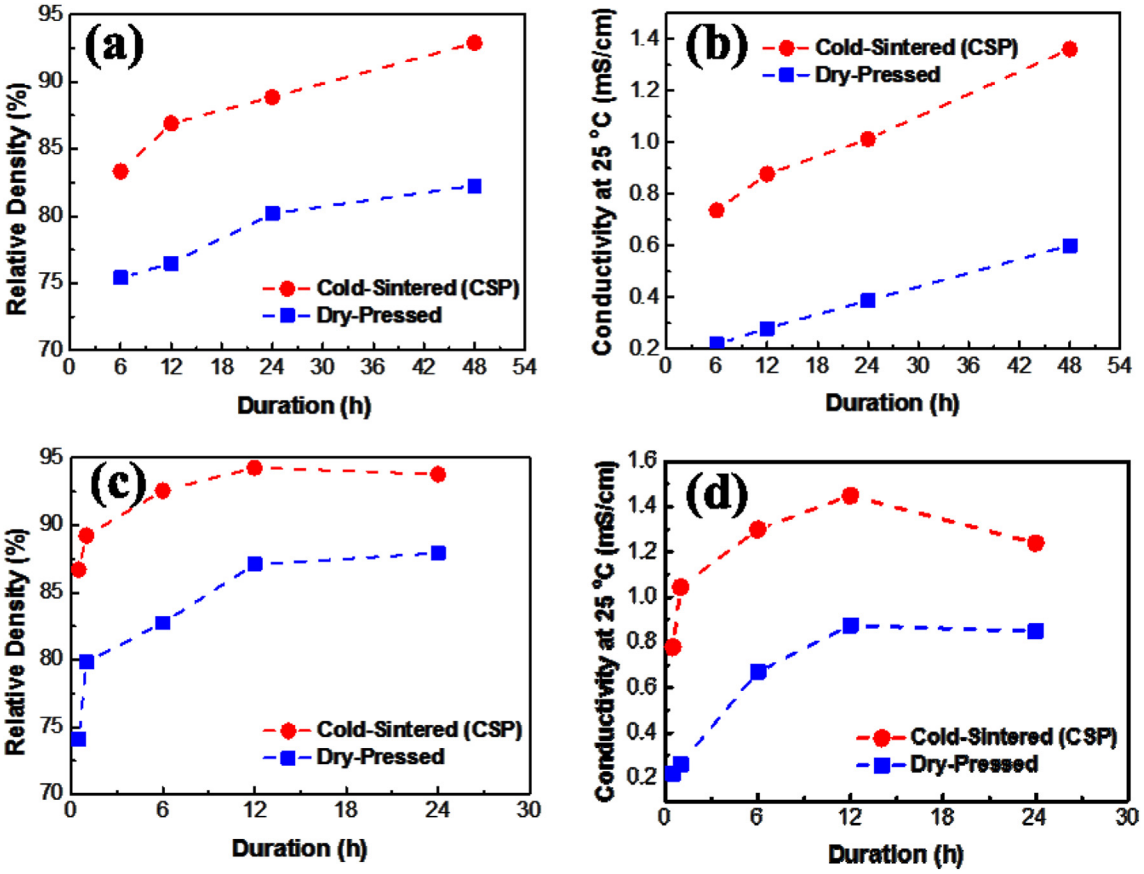

Fig. 5. Measured **(a, c)** relative density and **(b, d)** total room-temperature ionic conductivity of cold-sintered (CSP) and dry-pressed Mg-doped NASICON ($Na_{3.256}Mg_{0.128}Zr_{1.872}Si_2PO_{12}$) specimens vs. the duration for annealing at **(a, b)** 1100 °C and **(c, d)** 1150 °C, respectively. The estimated errors of measured densities are ± 1.5%.

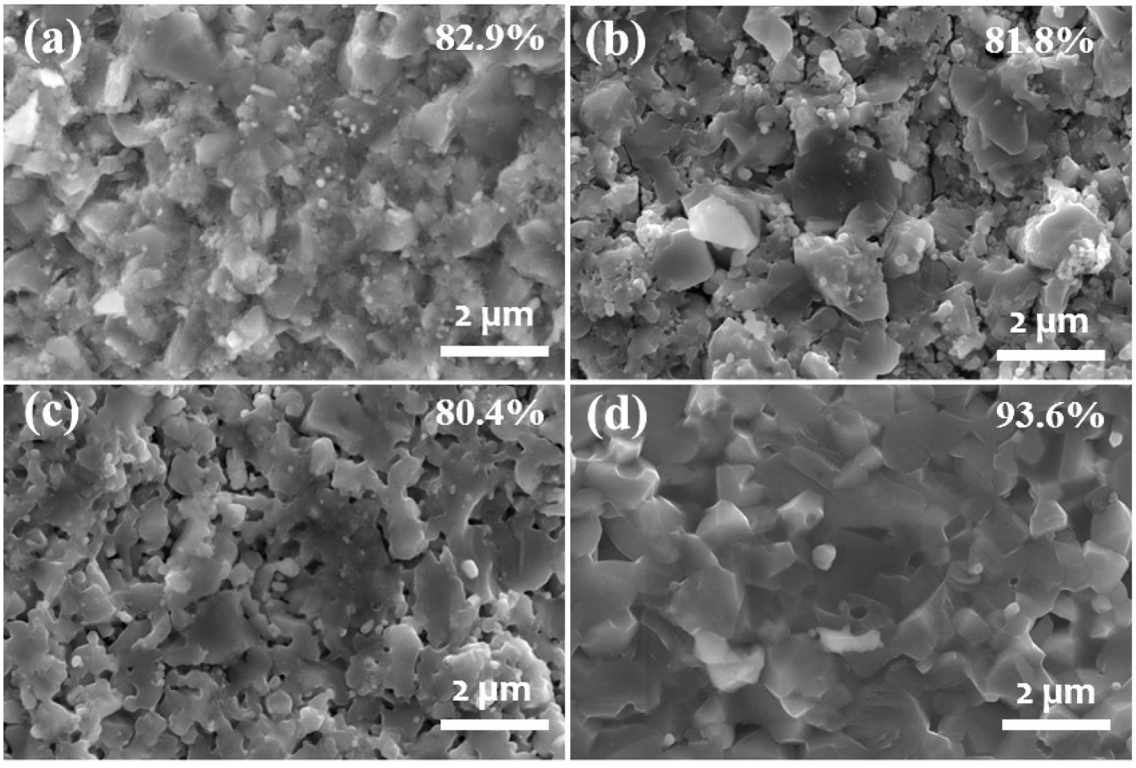

Fig. 6. SEM micrographs of the fractured surfaces of **(a)** as-cold-sintered (CSP only) specimens and cold-sintered Mg-doped NASICON ($Na_{3.256}Mg_{0.128}Zr_{1.872}Si_2PO_{12}$) specimens after subsequent annealing at **(b)** 800 °C for 6 h, **(c)** 900 °C for 6 h, and **(d)** 1100 °C for 48 h.

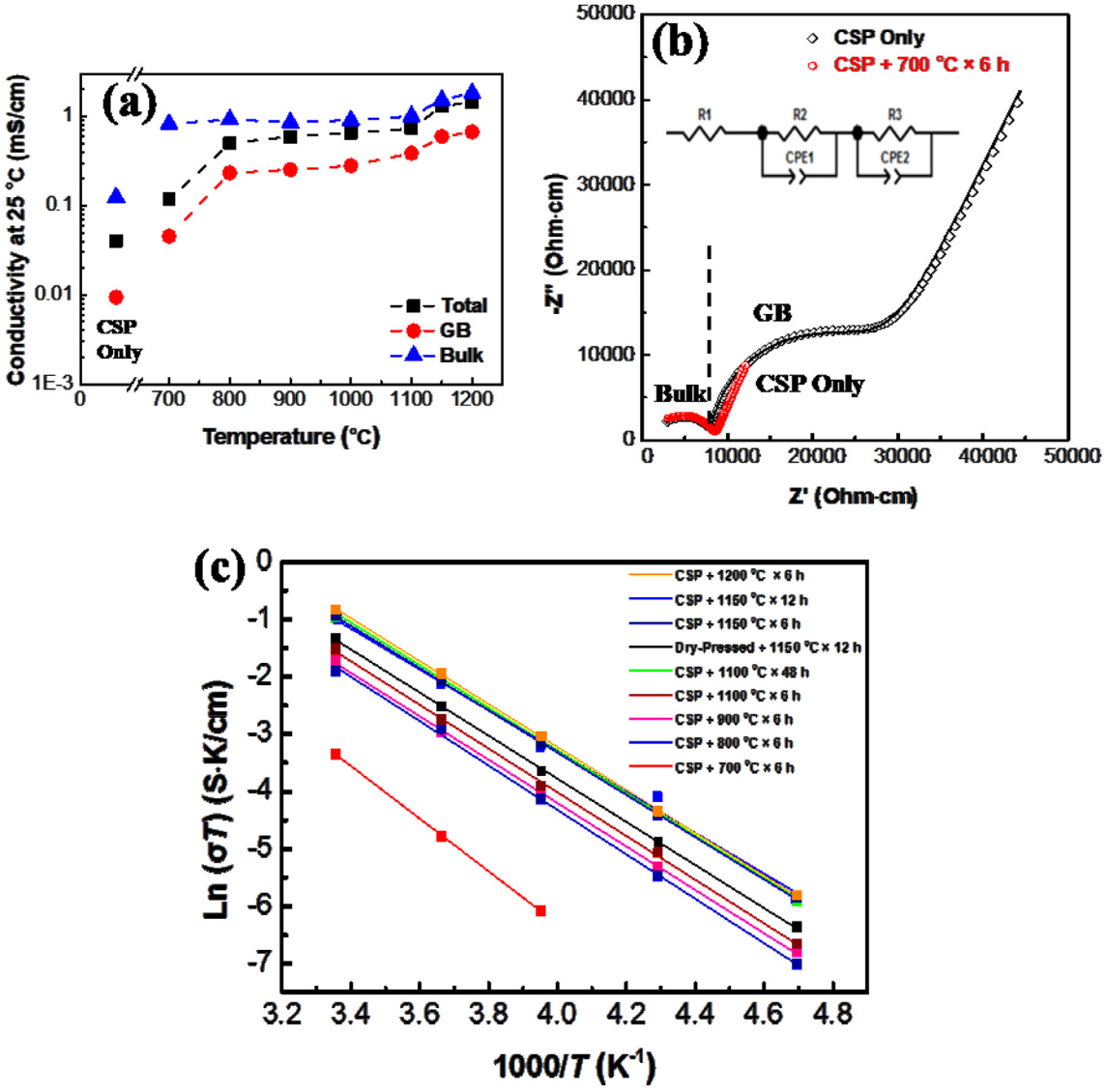

Fig. 7. (a) The total, GB, and bulk ionic conductivities (measured at room temperature) of cold-sintered Mg-doped NASICON ($Na_{3.256}Mg_{0.128}Zr_{1.872}Si_2PO_{12}$) specimens vs. annealing temperature curves. All specimens were annealed for 6 h. The measured total, GB, and bulk ionic conductivities of an as-cold-sintered specimen (CSP only) are also shown. **(b)** EIS plots (measured at 25 °C) of a CSP (only baked at 200 °C for 12 h) specimen and a CSP + 700 °C × 6 h specimen, along with corresponding fitted results (represented by the solid lines) using the equivalent circuit shown in the inset. **(c)** Arrhenius plots of the measured total conductivities of various Mg-doped NASICON specimens.

Table 2
Measured room-temperature GB (σ_{gb}), bulk (σ_b), and total (σ_t) conductivities for Mg-doped NASICON ($Na_{3.256}Mg_{0.128}Zr_{1.872}Si_2PO_{12}$) specimens cold-sintered (at 140 °C and 780 MPa for 1 h) and subsequently annealed at different temperatures.

Processing Condition	σ_{gb} (mS/cm)	σ_b (mS/cm)	σ_t (mS/cm)
As-CSP	0.009	0.125	0.041
CSP + 700 °C × 6 h	0.046	0.829	0.12
CSP + 800 °C × 6 h	0.233	0.924	0.529
CSP + 900 °C × 6 h	0.254	0.861	0.606
CSP + 1000 °C × 6 h	0.281	0.911	0.655
CSP + 1100 °C × 6 h	0.388	1.01	0.737
CSP + 1150 °C × 6 h	0.596	1.533	1.3
CSP + 1200 °C × 6 h	0.672	1.836	1.406

Mg-doped NASICON ($Na_{3.256}Mg_{0.128}Zr_{1.872}Si_2PO_{12}$) specimens cold-sintered at 140 °C for 1 h at 780 MPa, which was selected as the standard processing conditions for the subsequent experiments. The microstructures of a specimen cold-sintered with this set of conditions (140 °C, 1 h, 780 MPa) and a benchmark specimen dry-pressed at 780 MPa for 1 h are shown in Fig. 2 for comparison. Sintering morphologies, including particle packing and the formation on sintering necks, are evident in the cold sintered specimen. Mg doping was found effective and essential for promoting densification in cold sintering of NASICON, which also increased the conductivity of the specimen as discussed subsequently in §3.3.

3.2. The effects of Post-CSP annealing

Fig. 3 displays the XRD patterns of cold-sintered Mg-doped NASICON specimens before and after 6 h of annealing at 800, 900, 1000, 1100, 1150, and 1200 °C, respectively. All (both as-CSP and "CSP + annealing") specimens possess a primary crystalline NASICON phase similar to those reported previously [19–21]. Peaks from minor secondary phases, such as Na_3PO_4 and ZrO_2, are also labeled in Fig. 3. An unknown secondary phase was also identified in the specimens annealed at 1000 °C and 1100 °C. The presence of minor secondary phases is commonly found in sintered NASICON specimens [19–21].

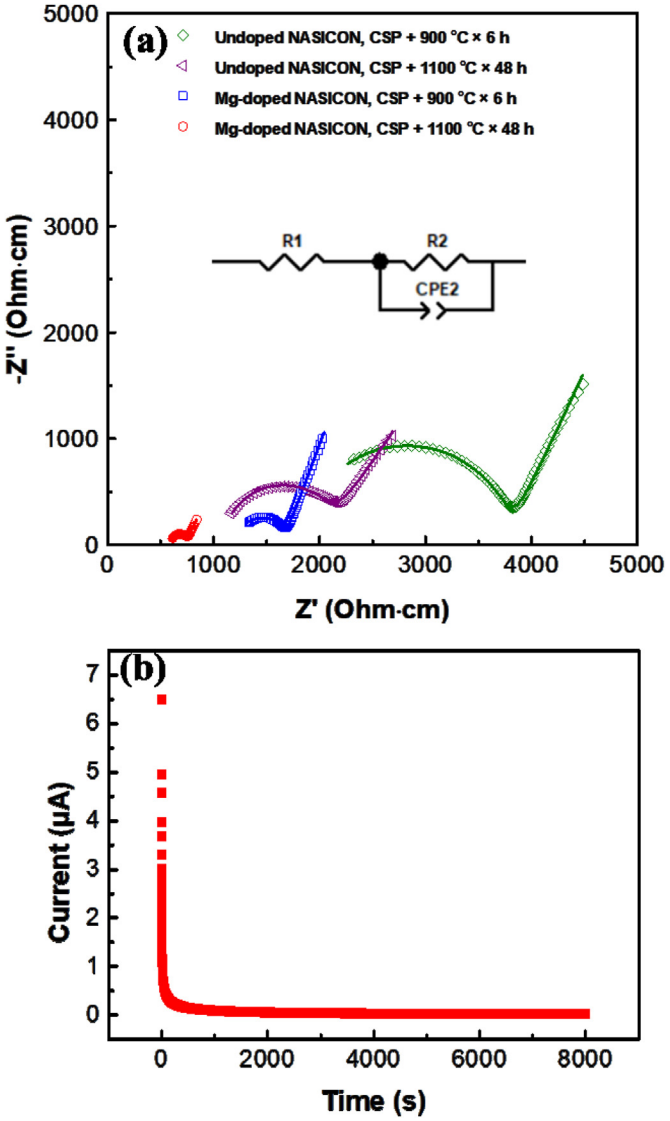

Fig. 8. (a) EIS plots (measured at 25 °C) of cold-sintered undoped ($Na_3Zr_2Si_2PO_{12}$) and Mg-doped ($Na_{3.256}Mg_{0.128}Zr_{1.872}Si_2PO_{12}$) NASICON specimens, respectively, annealed at 900 °C for 6 h and 1100 °C for 48 h, respectively along with corresponding fitted results (represented by the solid lines) using the equivalent circuit shown in the inset. **(b)** The DC polarization plot of a representative Mg-doped ($Na_{3.256}Mg_{0.128}Zr_{1.872}Si_2PO_{12}$) NASICON pellet (measured at 25 °C), indicating an ionic transfer number of > 0.997.

The effects of post-CSP annealing on improving the density and ionic conductivity of cold-sintered Mg-doped NASICON specimens were investigated (Fig. 4; Table 1). Dry-pressed specimens were also annealed (sintered) at the same conditions and the data are plotted together in Fig. 4 for comparison. Post-CSP annealing at 600–1000 °C had no appreciable effect on densification. Moderate densification occurred at 1100 °C (for 6 h), while a relative density of ~92.6% was achieved for 6 h annealing at 1150 °C (Fig. 4(a)). After annealing/sintering at the normal sintering temperature of 1200 °C for 6 h, ~98% of the theoretical density was obtained for both cold-sintered and dry-pressed specimens; we thereby concluded that the CSP would not provide much additional benefits when the normal sintering temperature is applied (but CSP can indeed provide substantial benefits at reduced sintering/annealing temperatures, in comparison with dry-pressed specimens). It is also interesting to note that the densities of cold-sintered NASICON specimens decreased slightly at 900–1000 °C, which may be related to the decomposition of the minor secondary phase(s) that may release small amounts of various gaseous species [36].

Fig. 4(b) shows the total ionic conductivities (measured at 25 °C) of both cold-sintered and dry-pressed Mg-doped NASICON ($Na_{3.256}Mg_{0.128}Zr_{1.872}Si_2PO_{12}$) specimens after annealing at different temperatures. Perhaps the most interesting result in Fig. 4 is that annealing at 800–1000 °C can substantially increase the conductivity despite of no significant increase in the specimen density. Specifically, the conductivity of cold-sintered Mg-doped NASICON reached > 0.5 mS/cm after annealing at as low as 800 °C for 6 h. Moreover, the total ionic conductivity of cold-sintered Mg-doped NASICON reached ~0.66 mS/cm at 1000 °C, which is eight times (8 ×) higher than that of the a dry-pressed specimen sintered at the identical condition (~0.08 mS/cm). The conductivity reached ~1.3 mS/cm at 1150 °C, which doubles the conductivity of the dry-pressed counterpart sintered at the identical condition (~0.67 mS/cm). However, the benefit of CSP became insignificant at the conventional sintering temperature of 1200 °C.

For a further critical comparison, a specimen was prepared by dry-pressing Mg-doped NASICON at 140 °C for 1h (without water addition) and subsequent annealing at 800 °C for 6 h. The measured density of this specimen was ~72.4% and the measured ion conductivity was ~0.075 mS/cm, which are only slightly higher than those of the specimen dry-pressed at room temperature and subsequently sintered at the identical condition (*i.e.*, ~70.3% density and ~0.061 mS/cm, respectively); however, these values are still substantially lower than those of the cold-sintered specimen sintered at the identical condition (*i.e.*, ~81.8% density and ~0.529 mS/cm, respectively). This additional comparison further and directly demonstrates that the water addition in CSP is essential to promote the densification of Mg-doped NASICON specimen.

We further investigated the variations of the density and ionic conductivity of both cold-sintered and dry-pressed Mg-doped NASICON specimens with the annealing duration at 1100 °C and 1150 °C, respectively. Both density and ionic conductivity increased with the increasing annealing duration (Fig. 5). Specifically, 30-min short annealing at 1150 °C can densify a cold-sintered specimen to ~86.7% to achieve a total conductivity of ~0.78 mS/cm, being significantly higher than the 74.1% relative density and ~0.22 mS/cm total conductivity of a dry-pressed specimen sintered at identical condition (Fig. 5(c)). Moreover, a high density of ~93% has been achieved for a cold-sintered Mg-doped NASICON specimen annealed at 1100 °C for 48 h (Fig. 5(a)) with high total ionic conductivity of ~1.36 mS/cm (Fig. 5(b)), which are substantially higher than those of a dry-pressed specimen sintered at the identical condition (i.e., ~82.3% density and ~0.60 mS/cm, respectively). While the densification and conductivity continued to increase with increasing annealing duration, at least up to 48 h, at 1100 °C, they both leveled off after ~12 h annealing at 1150 °C. Representative SEM images of the fractured surfaces of an as-CSP specimen as well as three cold-sintered specimens annealed at various temperatures are shown in Fig. 6.

To summarize the most significant observations, the total ionic conductivity of as-CSP specimen with ~82.8% density is only ~0.04 mS/cm, which can be increased by ~3 times to ~0.12 mS/cm after annealing at a temperature as low as 700 °C, or by > 10 times to ~0.53 mS/cm after annealing at a low temperature of 800 °C. These annealing temperatures are substantially lower than the conventional sintering temperature of NASICON, where no appreciable densification can occur. The underlying mechanisms were probed and discussed subsequently. Moreover, higher conductivities and densities can be achieved at higher annealing temperatures (e.g., ~0.8 mS/cm and ~87% density for a 30-min short annealing at 1150 °C or ~1.36 mS/cm and ~93% density for long annealing at a lower temperature of 1100 °C for 48 h), which are substantially higher than those can be achieved by conventional sintering of dry-pressed specimens at the same conditions (e.g., ~3.5 × and ~2 × higher conductivities in the above two examples, respectively). These discoveries suggest new opportunities for fabricating solid-state batteries, e.g., by co-firing

electrolytes and electrodes at reduced temperatures and/or shortened durations in one step. However, there will be trade-offs among processing temperature/duration and achievable conductivity/density. Yet, for example, fabrication of NASICON materials with a > 0.5 mS/cm conductivity without going beyond 800 °C is a new possibility unattainable previously, which can enable new fabrication routes for solid-state batteries.

3.3. The mechanisms of conductivity increases during low-temperature annealing

The enhancement of ionic conductivity of cold-sintered Mg-doped NASICON at 700–1000 °C cannot be explained by the density improvement, since there is essentially little or no densification (sintering) at 1000 °C or lower temperatures (Fig. 4). XRD studies did not reveal any significant changes in the primary NASICON phase (Fig. 3). Yet, the enhancement of total ionic conductivity started at 700 °C (by ~3 ×) and became substantial at 800 °C (to > 0.5 mS/cm, or a > 10 × increase from the as-CSP specimen). In contrast, the conductivity of a dry-pressed specimen sintered at 1000 °C for 6 h is only ~0.08 mS/cm, or only ~1/8th of the measured conductivity (~0.66 mS/cm) of a cold-sintered specimen annealed at the identical condition.

The heat treatment effects on ionic conductivity enhancement of other solid electrolytes have been investigated and attributed to crystallization of amorphous insulating phases at GBs in several prior studies [39–41]. The low ionic conductivity of cold-sintered NASICON specimens (despite achieving ~83% densities) could be related to the dissolution and precipitation of secondary phases (presumably with low crystallinity or being at least partially amorphous), which are known to form for NASICON in contact with water [42]. Small particles are evident on the surfaces of the NASICON grains (i.e., at GBs) in a fractured cold-sintered specimen in Fig. 6(a), which could be the secondary (amorphous or poorly-crystallized) phase precipitated around NASICON grains in the CSP; the numbers of similar small particles indeed reduced after annealing at 800 and 900 °C [Fig. 6(b–d)] and such small particles virtually disappeared after annealing at 1100 °C. Unfortunately, the exact composition of these small particles observed in Fig. 6(a) cannot be measured by energy-dispersive X-ray spectroscopy and NASICON is too beam sensitive for conducting high-resolution transmission electron microscopy (HRTEM). However, similar amorphous secondary and/or interfacial phases have been found in various other cold-sintered ceramics [30,32,34].

In addition, a prior study [21] showed that Mg doping enhanced the ionic conductivity of NASICON by promoting the formation of more conductive secondary Na_3PO_4 phase, which were also found in our specimens (Fig. 3). Moreover, Na_3PO_4 can transform from a tetragonal α phase to a cubic γ phase at ~600 °C with a jump in its ionic conductivity [43]. The enhancement of ionic conductivity of γ-Na_3PO_4 with a cubic structure is attributed to the increased number of mobile Na^+ vacancies [44]. Thus, this α-to-γ phase transformation in the secondary Na_3PO_4 phase, in addition to possible crystallization of the secondary amorphous (or poorly-crystallized) phase, may contribute to the observed increased (mostly GB, instead of the bulk) conductivity of our cold-sintered specimens during annealing at 700–1000 °C. Unfortunately, the amount of the secondary phase is too small for examining its structure or crystallinity directly with XRD, and NASICON is too beam sensitive for HRTEM (as the intense beam in HRTEM would amorphize the specimen in seconds).

To test the hypothesized mechanisms, we separate the GB conductivities and bulk conductivities by fitting EIS plots with a brick layer model [45]; the results are shown in Fig. 7(a) and Table 2. It is noticed that the bulk conductivity is always higher than the GB conductivity in all specimens, which indicates the total ionic conductivity is mostly limited by the high GB resistance. Specifically, annealing at 700 °C substantially increased both bulk and GB conductivities. Fig. 7(b) displays the impedance spectra of the cold-sintered Mg-doped NASICON specimens before and after annealing at 700 °C, where the two semicircles of the EIS plots correspond to bulk and GB resistances [46]. An equivalent circuit model (as shown in the inset in Fig. 7(b)) with two R-CPE components to represent the bulk and grain boundary contributions, respectively, was used for data fitting.

Notably, the bulk conductivities of specimens annealed at 700–1000 °C are essentially the same [Fig. 7(a)]. Annealing at 800 °C further increased (only) the GB conductivity substantially in comparison with that of the specimen annealed at 700 °C (while there is essentially no difference in the bulk conductivities). Furthermore, annealing at higher temperatures 900 and 1000 °C, respectively, increased the total conductivity slightly by modestly increasing (only) the GB conductivity. Finally, both bulk and GB conductivities increased after annealing at high temperatures of 1100–1200 °C. Arrhenius plots of the measured conductivities of various Mg-doped NASICON specimens are shown in Fig. 7(c).

These observations are largely consistent with the above-discussed hypothesis that annealing at 800–1000 °C increased the total conductivity substantially [Fig. 4(b)] mostly through increasing the GB conductivity [Fig. 7(a)] via (presumably) crystallization of secondary and interfacial amorphous (or poorly-crystallized) phase(s) and/or the α-to-γ phase transformation in the secondary Na_3PO_4 phase.

Finally, we also compared the measured conductivities of cold-sintered undoped vs. Mg-doped NASICON specimens (Table 1; Fig. 8(a), where the equivalent circuit model is shown in the inset in Fig. 8(a)). It is noticed that Mg doping substantially increased the total ionic conductivity in all cases. For example, the measured total ionic conductivities of the cold-sintered undoped and Mg-doped NASICON specimens, respectively, after 900 °C × 6 h annealing are ~0.27 mS/cm and ~0.61 mS/cm, respectively. Moreover, the measured total ionic conductivities of the cold-sintered undoped and Mg-doped NASICON specimens, respectively, after 1100 °C × 48 h annealing are ~0.51 mS/cm and ~1.36 mS/cm, respectively. In both cases, Mg doping increased the total conductivities by more than 2 ×. As demonstrated by a prior coupled experimental and modeling study [21], Mg doping can increase GB conductivities by forming a conductive secondary and/or interfacial Na_3PO_4 phase at the NASICON GBs, which are consistent with the current observations using cold-sintered specimens (Figs. 3 and 8(a)). Fig. 8(b) further shows the DC polarization plot of a representative $Na_{3.256}Mg_{0.128}Zr_{1.872}Si_2PO_{12}$ pellet, where the sodium ion transfer number was measured to be > 0.997, verifying that the conductivity of the specimen is mostly ionic.

4. Conclusions

Mg-doped NASICON ($Na_{3.256}Mg_{0.128}Zr_{1.872}Si_2PO_{12}$) specimens were cold sintered at 140 °C to ~ 83% of the theoretical density. Subsequent low-temperature annealing at 800 °C can help to substantially increase the conductivity by mostly increasing the GB conductivity to achieve is > 0.5 mS/cm. In contrast, a dry-pressed specimen exhibited virtually no densification at a higher sintering temperature of 1000 °C and a much lower conductivity of < 0.1 mS/cm. Moreover, 30-min short annealing at 1150 °C of the cold-sintered specimen can achieve ~87% density and ~0.8 mS/cm conductivity, in comparison with ~74% density and ~0.2 mS/cm conductivity of a dry-pressed specimen sintered at the identical condition. A high density of ~93% and higher total ionic conductivity of ~1.36 mS/cm have been achieved for a cold-sintered Mg-doped NASICON specimen, in comparison with ~82% density and ~0.6 mS/cm of a dry-pressed specimen, after annealing/sintering at the identical condition of 1100 °C × 48 h. These discoveries suggest new opportunities/routes for fabricating solid-state batteries, e.g., by co-firing electrolytes and electrodes at reduced temperatures and/or shortened durations, where trade-offs among processing temperature/duration and achievable conductivity/density should be made. The successful fabrication of NASICON materials with a > 0.5 mS/cm conductivity without going beyond 800 °C, for example,

represents a new possibility and enabling capability that have not been achieved before. In a broader context, the CSP technology provides a new opportunity to sinter the "thermally-fragile" ceramic solid electrolytes for both Li^+ and Na^+ (such as phosphates and sulfates with volatile components and prone to the decomposition and/or precipitation of harmful secondary phases at high temperatures), and it can also provide significant energy and cost savings.

Acknowledgement

This work was partially supported by a Vannevar Bush Faculty Fellowship sponsored by the Basic Research Office of the Assistant Secretary of Defense for Research and Engineering and funded by the Office of Naval Research through grant no. N00014-16-1-2569. J. N. is supported by the Aerospace Materials for Extreme Environments program of the Air Force Office of Scientific Research (AFOSR) under the grant no.FA9550-14-1-0174 and J.N. and J.L. also thank the AFOSR program manager, Dr. Ali Sayir, for his support and guidance.

References

[1] K.B. Hueso, M. Armand, T. Rojo, Energy Environ. Sci. 6 (2013) 734–749.
[2] B.L. Ellis, L.F. Nazar, Curr Opin Solid St M 16 (2012) 168–177.
[3] Z.L. Jian, W.Z. Han, X. Lu, H.X. Yang, Y.S. Hu, J. Zhou, Z.B. Zhou, J.Q. Li, W. Chen, D.F. Chen, L.Q. Chen, Adv Energy Mater 3 (2013) 156–160.
[4] P. Senguttuvan, G. Rousse, V. Seznec, J.M. Tarascon, M.R. Palacin, Chem. Mater. 23 (2011) 4109–4111.
[5] Z.Z. Zhang, Q.H. Zhang, J.A. Shi, Y.S. Chu, X.Q. Yu, K.Q. Xu, M.Y. Ge, H.F. Yan, W.J. Li, L. Gu, Y.S. Hu, H. Li, X.Q. Yang, L.Q. Chen, X.J. Huang, Adv Energy Mater 7 (2017).
[6] E. Quartarone, P. Mustarelli, Chem. Soc. Rev. 40 (2011) 2525–2540.
[7] F. Lalere, J.B. Leriche, M. Courty, S. Boulineau, V. Viallet, C. Masquelier, V. Seznec, J. Power Sources 247 (2014) 975–980.
[8] C. Zhao, L. Liu, X. Qi, Y. Lu, F. Wu, J. Zhao, Y. Yu, Y.S. Hu, L. Chen, Adv Energy Mater 2018 (2018) 1703012.
[9] W.D. Zhou, Y.T. Li, S. Xin, J.B. Goodenough, Acs Central Sci 3 (2017) 52–57.
[10] V. Palomares, P. Serras, I. Villaluenga, K.B. Hueso, J. Carretero-Gonzalez, T. Rojo, Energy Environ. Sci. 5 (2012) 5884–5901.
[11] D. Kundu, E. Talaie, V. Duffort, L.F. Nazar, Angew. Chem. Int. Ed. 54 (2015) 3431–3448.
[12] K. Hayashi, K. Shima, F. Sugiyama, J. Electrochem. Soc. 160 (2013) A1467–A1472.
[13] Z.Z. Zhang, K.Q. Xu, X.H. Rong, Y.S. Hu, H. Li, X.J. Huang, L.Q. Chen, J. Power Sources 372 (2017) 270–275.
[14] J.K. Kim, Y.J. Lim, H. Kim, G.B. Cho, Y. Kim, Energy Environ. Sci. 8 (2015) 3589–3596.
[15] Z.Z. Zhang, Q.Q. Zhang, C. Ren, F. Luo, Q. Ma, Y.S. Hu, Z.B. Zhou, H. Li, X.J. Huang, L.Q. Chen, J. Mater. Chem. 4 (2016) 15823–15828.
[16] H.Y.P. Hong, Mater. Res. Bull. 11 (1976) 173–182.
[17] J.B. Goodenough, H.Y.P. Hong, J.A. Kafalas, Mater. Res. Bull. 11 (1976) 203–220.
[18] J.W. Fergus, Solid State Ionics 227 (2012) 102–112.
[19] A.G. Jolley, G. Cohn, G.T. Hitz, E.D. Wachsman, Ionics 21 (2015) 3031–3038.
[20] S.F. Song, H.M. Duong, A.M. Korsunsky, N. Hu, L. Lu, Sci Rep-Uk 6 (2016).
[21] M. Samiee, B. Radhakrishnan, Z. Rice, Z. Deng, Y.S. Meng, S.P. Ong, J. Luo, J. Power Sources 347 (2017) 229–237.
[22] S. Song, H.M. Duong, A.M. Korsunsky, N. Hu, L. Lu, Sci Rep-Uk 6 (2016) 32330.
[23] Q. Ma, M. Guin, S. Naqash, C.-L. Tsai, F. Tietz, O. Guillon, Chem. Mater. 28 (2016) 4821–4828.
[24] S. Chen, C. Wu, L. Shen, C. Zhu, Y. Huang, K. Xi, J. Maier, Y. Yu, Adv. Mater. 29 (2017) 1700431.
[25] A.G. Jolley, G. Cohn, G.T. Hitz, E.D. Wachsman, Ionics 21 (2015) 3031–3038.
[26] J.S. Lee, C.M. Chang, Y.I. Lee, J.H. Lee, S.H. Hong, J. Am. Ceram. Soc. 87 (2004) 305–307.
[27] A. Ahmad, T.A. Wheat, A.K. Kuriakose, J.D. Canaday, A.G. Mcdonald, Solid State Ionics 24 (1987) 89–97.
[28] J.P. Maria, X.Y. Kang, R.D. Floyd, E.C. Dickey, H.Z. Guo, J. Guo, A. Baker, S. Funihashi, C.A. Randall, J. Mater. Res. 32 (2017) 3205–3218.
[29] S. Funahashi, J. Guo, H.Z. Guo, K. Wang, A.L. Baker, K. Shiratsuyu, C.A. Randall, J. Am. Ceram. Soc. 100 (2017) 546–553.
[30] H.Z. Guo, J. Guo, A. Baker, C.A. Randall, Acs Appl Mater Inter 8 (2016) 20909–20915.
[31] H.Z. Guo, J. Guo, A. Baker, C.A. Randall, J. Am. Ceram. Soc. 100 (2017) 491–495.
[32] H.Z. Guo, T.J.M. Bayer, J. Guo, A. Baker, C.A. Randall, J. Eur. Ceram. Soc. 37 (2017) 2303–2308.
[33] H.Z. Guo, A. Baker, J. Guo, C.A. Randall, J. Am. Ceram. Soc. 99 (2016) 3489–3507.
[34] J. Guo, H.Z. Guo, D.S.B. Heidary, S. Funahashi, C.A. Randall, J. Eur. Ceram. Soc. 37 (2017) 1529–1534.
[35] J.H. Seo, J. Guo, H.Z. Guo, K. Verlinde, D.S.B. Heidary, R. Rajagopalan, C.A. Randall, Ceram. Int. 43 (2017) 15370–15374.
[36] S.S. Berbano, J. Guo, H.Z. Guo, M.T. Lanagan, C.A. Randall, J. Am. Ceram. Soc. 100 (2017) 2123–2135.
[37] R.O. Fuentes, F. Figueiredo, F.M.B. Marques, J.I. Franco, Solid State Ionics 139 (2001) 309–314.
[38] M. Guin, S. Indris, M. Kaus, H. Ehrenberg, F. Tietz, O. Guillon, Solid State Ionics 302 (2017) 102–106.
[39] P. Johnson, N. Sammes, N. Imanishi, Y. Takeda, O. Yamamoto, Solid State Ionics 192 (2011) 326–329.
[40] C.R. Mariappan, C. Yada, F. Rosciano, B. Roling, J. Power Sources 196 (2011) 6456–6464.
[41] V. Thangadurai, W. Weppner, J. Solid State Chem. 179 (2006) 974–984.
[42] F. Mauvy, E. Siebert, P. Fabry, Talanta 48 (1999) 293–303.
[43] A. Ghule, N. Baskaran, R. Murugan, H. Chang, Solid State Ionics 161 (2003) 291–299.
[44] J.T.S. Irvine, A.R. West, Mater. Res. Bull. 22 (1987) 1047–1054.
[45] H. Chung, B. Kang, Solid State Ionics 263 (2014) 125–130.
[46] X.X. Xu, Z.Y. Wen, Z.H. Gu, X.H. Xu, Z.X. Lin, Solid State Ionics 171 (2004) 207–213.